International Journal of Fracture 29 (1985) 113–124.

Elastic-plastic analysis and J-dominance of the double punch mode II fracture toughness specimen

R. BRADFORD

Central Electricity Generating Board, South Western Region, Bedminster Down, Bristol, England

(Received March 21, 1985)

Abstract

The elastic-plastic finite element program BERSAFE Phase 3 is used to analyse the Double Punch specimen. The validity of mode II toughnesses obtained from this specimen for loads beyond general yield is investigated by examining the near crack tip fields for J-dominance. These fields are found to be consistent with the mode II HRR fields. In addition, the eta factors correlating J with the work done on the specimen, U, are found, and this provides the simplest means of experimental toughness measurement. Finally, the J calculations are expressed in an assessment diagram format although the applicability of this diagram to structural geometries is not investigated. The analyses assume plane stress constraint and stress-strain data obtained from a carbon-manganese steel.

1. Introduction

In recent years the J-integral has become an accepted measure of the toughness of ductile materials. From the theoretical point of view, the strength of the case for regarding J as an appropriate fracture parameter derives from its ability to uniquely characterise the crack tip fields. Thus, for a given material behaviour, and for loading in a fixed mode, the J-integral uniquely defines the crack tip stress and strain fields regardless of the geometry of the structure/specimen or of the crack, provided the relevant dimensions exceed certain limits expressed as multiples of $J/\mathcal{O}_0$. For mode I specimen geometries, these "validity criteria" have been discussed by McMeeking and Parks [1], Shih and German [2] and Needleman and Tvergaard [3]. In the present paper we turn our attention to mode II (in-plane shear). Green and Miles [4] have described the use of a Double Punch Specimen (DPS) to determine mode II toughnesses in the post-yield regime. An elastic-plastic finite element analysis of the DPS is carried out here in order to investigate the validity of toughnesses measured in this way. Since carbon-manganese steel was the subject of the investigations of [4], material behaviour characteristic of mild steel is assumed in the finite element analysis. An earlier paper, [5], has performed a similar analysis for an edge cracked square plate in pure mode II shear with $n = 3$ power law hardening.

2. Description of Double Punch specimen

The specimens employed in [4] were Charpy sized specimens with a 1 cm × 1 cm section. Two cracks were spark machined symmetrically, 20 mm apart. The specimen is loaded in a rig which tightly clamps the ends and allows a descending punch to extrude the centre, as

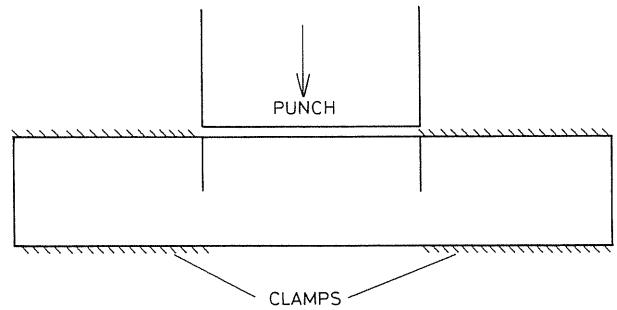

Figure 1. The Double Punch Specimen.

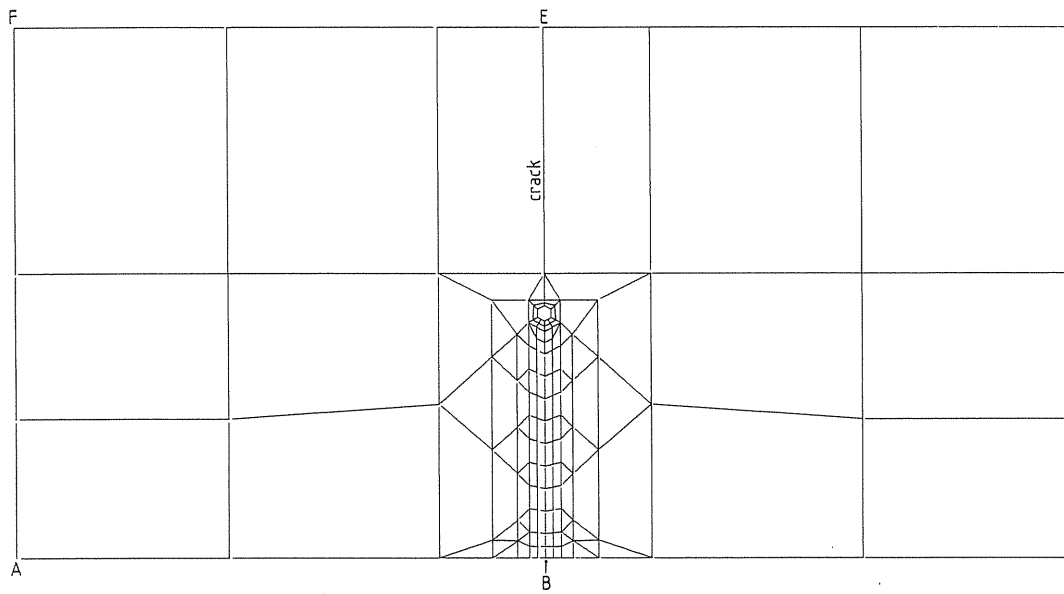

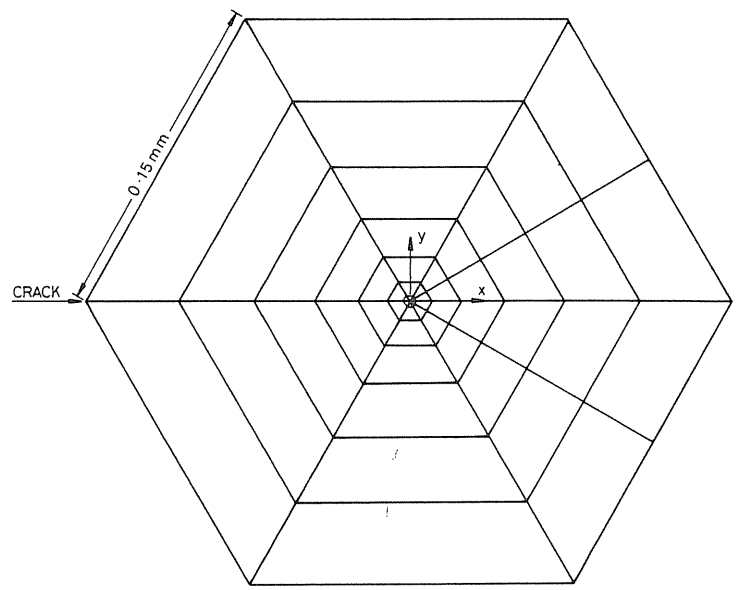

Figure 2. (a) Mesh, (b) Mesh detail.

shown in Fig. 1. Any mode I loading induced by bending is minimised by working to a close tolerance between the clamped and punched regions.

3. The finite element model

Because of symmetry about the midplane, only half the specimen need be modelled. The 2-dimensional mesh is shown in Fig. 2(a), the crack tip being at the centre of the hexagon. The specimen width, W, is 10 mm and the mesh thickness B is taken as 1 mm. Two crack lengths were analysed, $a = 5$ and $a = 5.385$ mm. The refined hexagonal region/about the crack tip is shown in Fig. 2(b).

Loading is achieved by:

(a) Fixing edges EF and AB in Fig. 2(a) in both directions.
(b) Fixing CD in its normal direction (the symmetry condition).
(c) Applying a uniform downward displacement to face DE.

Plane stress constraint was assumed. It is debatable whether plane stress or plane strain constraint is the better approximation to the actual specimen behaviour. Ideally, a 3-dimensional analysis would be desirable to avoid such simplifications but this is impracticable with the level of refinement needed to calculate the near tip fields. A previous paper, [5], has considered plane strain behaviour in mode II.

The elastic data assumed in the analysis was $E = 210$ GPa and $\nu = 0.3$. The post-yield stress-strain behaviour shown in Fig. 3 was input to the computer program as a discrete set of points. This is the true stress/true strain curve at ambient temperature for a carbon-manganese steel of the type used by Green and Miles [4]. The present work differs from most analyses of this type in employing real material data rather than idealised power-law hardening. The limit of proportionality occurs at 0.1% strain, and stress $\mathcal{O}_0 = 210$ MPa. The 0.2% permanent set (proof) stress is $\mathcal{O}_y = 255$ MPa, and the engineering ultimate stress $\mathcal{O}_u = 429$ MPa.

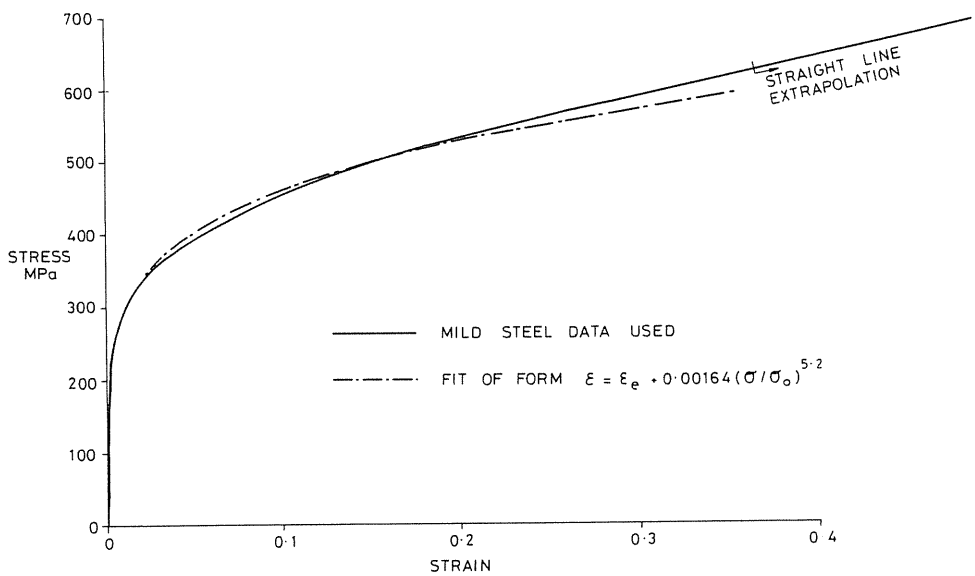

Figure 3. Stress-strain data.

The finite element program employed was BERSAFE Phase 3 (Level 1) [6]. This is based on incremental flow theory and infinitesimal strain/displacement theory. The latter is consistent with the small scale yielding fields of Hutchinson [7] and Rice and Rosengren [8] (henceforth called the HRR fields) whose analyses also assumed small strain behaviour. In reality, sufficiently near the crack tip, the fields will certainly be influenced by crack tip geometry changes in the post-yield regime. It seems probable, however, that observation of the HRR fields in an infinitesimal strain analysis is sufficient to imply J-dominance of the near tip, finite strain fields. In any case, conclusions drawn from infinitesimal strain analyses regarding specimen validity implicitly make this assumption. Finally, the analysis uses the von-Mises yield criterion and isotropic hardening.

4. Loading record and calculation of J

Both crack lengths were analysed up to an applied displacement of 45 μm in 90 equal increments, each increment involving many iterations (typically 10 to 20). The analysis of the smaller crack length ($a/W = 0.5$) was extended to a total of 61 μm in a further 45 increments at which point convergence problems were encountered and analysis had to be discontinued. The load-displacement behaviour resulting from the analyses is shown in Fig. 4. These load-displacement data were fitted to a 7th order polynomial. The mean of the two fits is shown as the continuous line in Fig. 4. The difference of the two fits allows the difference in the work done ΔU between the two crack lengths, at a given displacement D, to be calculated by explicit integration. J is then calculated through its interpretation as the energy release rate, $-\Delta U/B\Delta a$. The results are also shown in Fig. 4. The LEFM value for J is also shown for comparison at *the same displacement* (the load axis does not apply to the LEFM value). These results apply to the average crack length, i.e. $a/W = 0.519$. The normalised elastic stress intensity factor ($K/\tau\sqrt{\pi a}$) was found to be 1.00, where $\tau = F/BW$ and F is the load applied to the mesh.

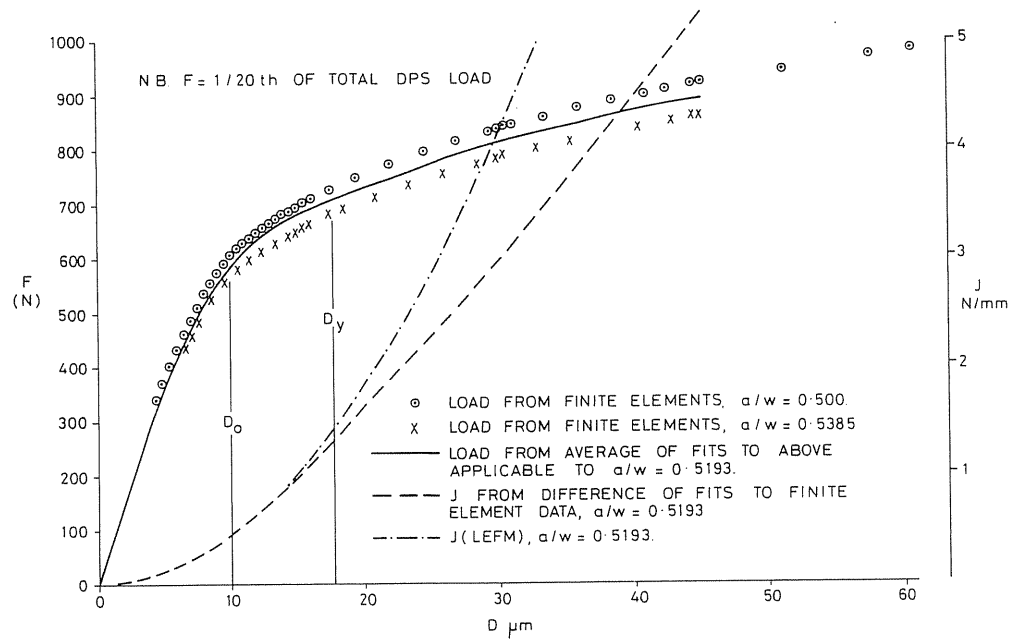

Figure 4. Load-displacement and J-displacement curves.

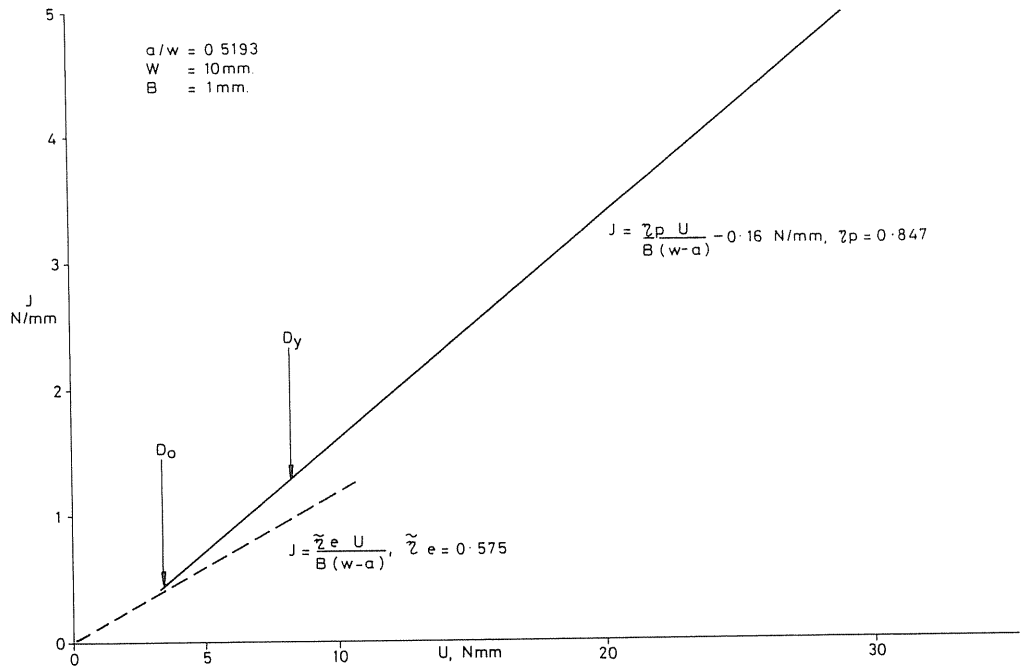

Figure 5. Plot of J versus U.

Figure 5 plots J against the work done, U. Experimenters often employ J-estimation formulae which relate J linearly to U. Figure 5 shows this to be justified for the DPS beyond general yielding and gives the "eta factor" $\eta_P = 0.847$, where,

$$J = \frac{\eta_P U}{B(W-a)} - 0.16 \text{ N/mm} \quad \text{(beyond general yield)} \tag{1}$$

(Note: U is the total work done, including the elastic part).

Thus, the effect of the strain hardening is to reduce η_P below the value of unity that would be expected from a simple, perfectly plastic limit load analysis. Evidence in support of this

Table 1. ETA factors

D (μm)	Estimation of Ref. [9]	Present analysis
≤ 6	0.575 *	0.575 *
15	0.78	0.73
25	0.83	0.79
35	0.86	0.81
45	0.87	0.82
100	0.91	–
200	0.93	–
300	0.94	–
400	0.94	–
∞	1	–

* LEFM value

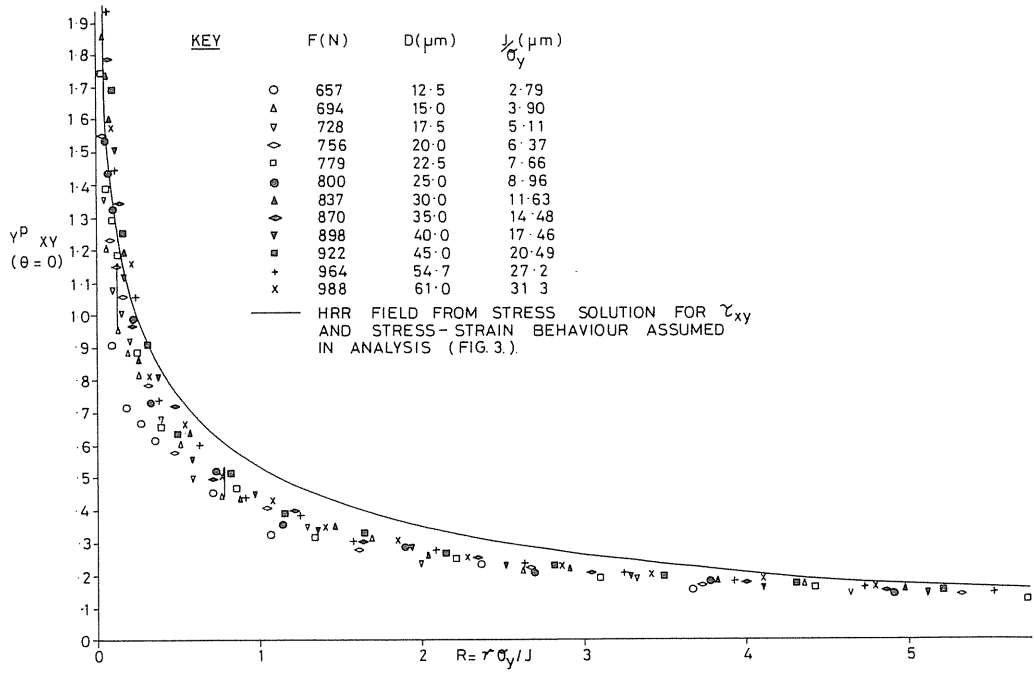

Figure 6. Plastic engineering shear strain on ligament ($\theta = 0$) against normalised distance from crack tip.

may be obtained by using the J-estimation procedure of Bradford [9]. This procedure interpolates,

$$\eta = \frac{JB(W-a)}{U} \tag{2}$$

between the LEFM and limit load regimes. The results of this procedure are compared with the results of the finite element analyses in Table 1. The two methods are broadly in agreement, and the estimation procedure shows η tending asymptotically to 1 for large D.

In Figs. 4 and 5, D_0 and D_y are the displacements at which the mean ligament shear stress, $\tau_L = F/B\ (W-a)$, for the average crack length, is $\tau_0 = \mathcal{O}_0/\sqrt{3}$ and $\tau_y = \mathcal{O}_y/\sqrt{3}$ respectively. General yielding occurred very close to displacement D_0, i.e. when the mean ligament shear stress was τ_0. This contrasts with the plane strain, square plate analysis of [5] for which general yielding did not occur until the mean ligament shear was 1.36 τ_0. Figure 4 shows that, for the same displacement, the LEFM and elastic-plastic values for J are equal for loads up to general yielding, or slightly beyond. This was also observed in [5].

5. Crack tip fields

In plotting the crack tip fields we make use of a dimensionless distance $R = r\mathcal{O}_y/J$. J-dominance of the tip fields is then characterised by a unique curve against R at all loads. Figures 6 and 7 show the (engineering) shear strain and shear stress on the ligament (i.e. $\theta = 0$) within $R \sim 5$ in the general yield regime. The FE data cover an 11-fold increase in J, all beyond general yield, and all fall fairly convincingly on a single curve, barring some numerical noise. Shih [10] has calculated the HRR fields for mode II in plane stress and for power law hardening with $n = 3$ and $n = 13$. On $\theta = 0$ the HRR amplitude factors are the same for $n = 3$ and $n = 13$ (see Table 2) and may be taken to be appropriate for the present materials data for which a power law fit gives $n = 5.2$. The HRR shear stress

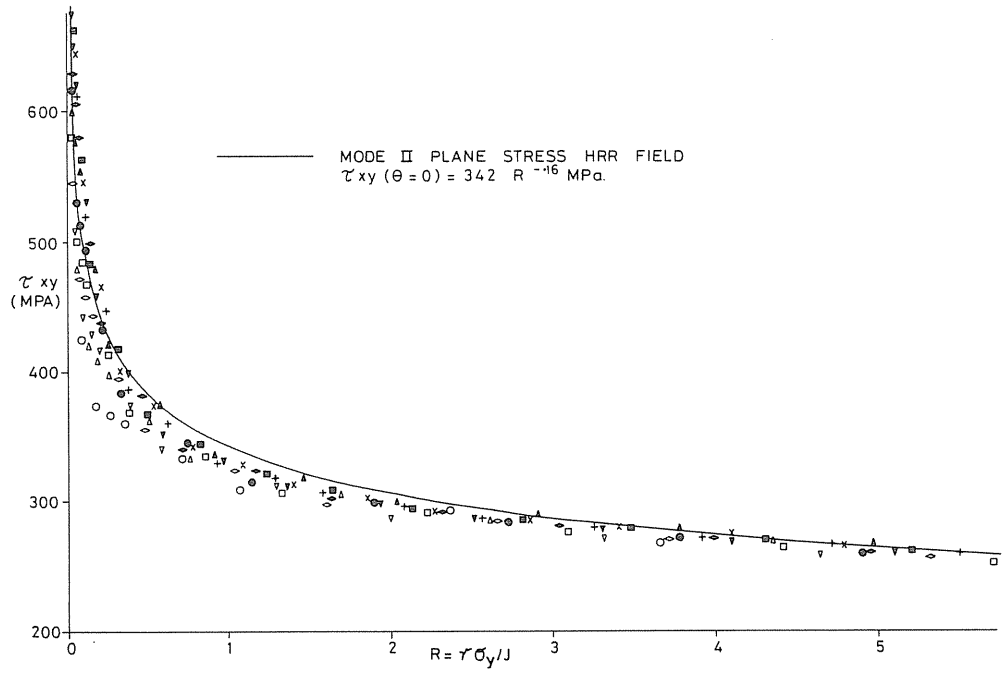

Figure 7. Shear stress on ligament ($\theta = 0$) versus normalised distance from crack tip.

on the ligament is therefore derived to be 342 $R^{-0.16}$ MPa. This curve is shown in Fig. 7 and compares well with the finite element results in general yield. Because a power law behaviour was not assumed in our analysis, care must be taken in deriving the "HRR" strain field to compare with our *FE* results. Essentially this is because the best power law fit to our data may give significantly different strains from the data assumed in the analysis at strain levels above those plotted in Fig. 3. (BERSAFE uses a linear extrapolation beyond the last two input data points). The simplest strain "prediction" is obtained by combining our assumed materials data with the above HRR stress field. The result is shown in Fig. 6 and is in reasonably good agreement with the *FE* results.

Figures 8 and 9 give the θ components of strain and stress respectively on the radial line at $\theta = 60°$ to the ligament. The data again lies on a unique curve at all loads, to within some numerical tolerance, indicating J-dominance. In this case the mode II, plane stress HRR fields from [10] have differing amplitude factors for $n = 3$ and $n = 13$ (see Table 2). Figures 8 and 9 include HRR "predictions" based on both these amplitude factors, but using the radial dependence and I_n factor appropriate to $n = 5.2$ (best fit) in every case. The two HRR curves roughly define upper and lower bounds to our *FE* results, indicating agreement to within the best accuracy that can be established with existing HRR solutions.

Table 2. HRR parameters used (mode II, plane stress)

θ	Amplitude parameter
0	$\mathcal{O}^3_{XY} = \mathcal{O}^{13}_{XY} = 0.57$
60°	$\epsilon^3_\theta = 0.43, \quad \epsilon^{13}_\theta = 0.18$
60°	$\mathcal{O}^3_\theta = 0.77, \quad \mathcal{O}^{13}_\theta = 0.90$

All radial functions defined by $n = 5.2$
$I_{5.2} = 1.1, \ \alpha = 1.64$

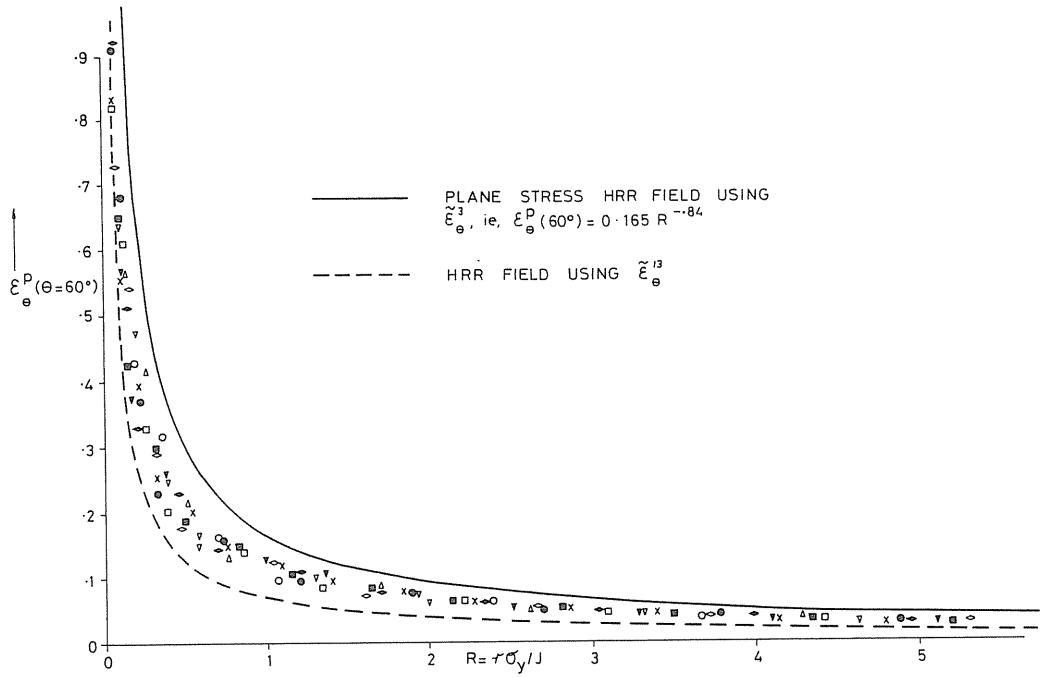

Figure 8. Plastic θ-strain on $\theta = 60°$ versus normalised distance.

Finally, Fig. 10 plots the engineering shear strain on the ligament against R on a logarithmic scale. For HRR behaviour, the resulting plot should be a straight line with slope 0.84. The *FE* data is indeed of this form, up to a maximum distance somewhat in excess of 1 mm.

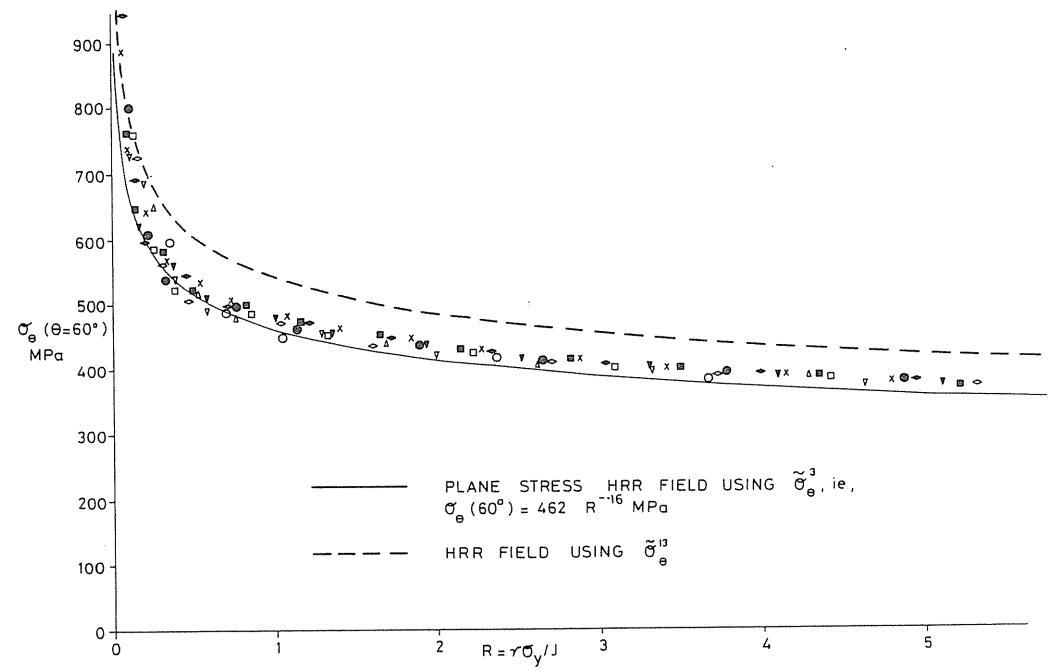

Figure 9. θ-stress on $\theta = 60°$ versus normalised distance.

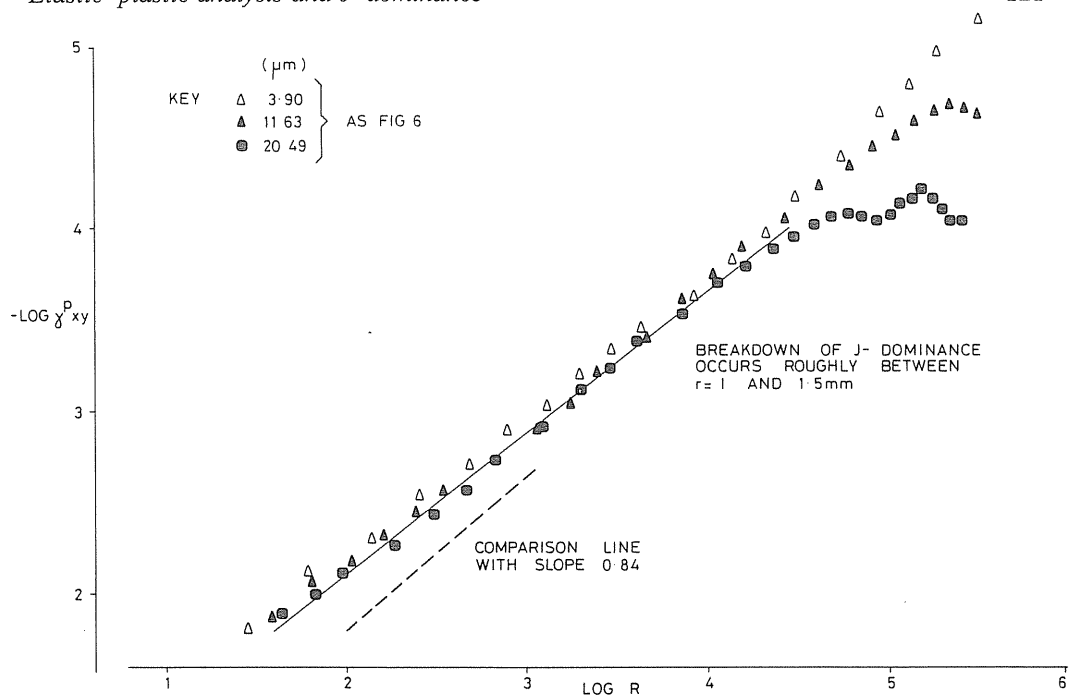

Figure 10. Log plot of plastic shear strain on ligament ($\theta = 0$, $R > 5$).

6. Assessment diagram

The results of an elastic-plastic calculation of J may be expressed in the format of an assessment diagram. This is achieved by defining the ordinate,

$$K_r = \sqrt{\frac{J(\text{LEFM})}{J(\text{elastic-plastic})}}$$

The numerator and denominator being evaluated at the same load (F), so that $K_r \lesssim 1$. An assessment diagram plots K_r against a suitably normalised load. We choose as abscissa.

$$S_r = \frac{\tau_L}{\tau_f}, \quad \tau_f = \frac{\mathcal{O}_y + \mathcal{O}_u}{2\sqrt{3}}$$

Values of S_r and K_r are given in Table 3 and presented graphically in Fig. 11. For comparison, the assessment diagram of Bradford et al, [11], derived from (mode I) compact tension specimens using the same material data (see Fig. 3) is also shown in Fig. 11. Note that the definition of S_r implies that if collapse is associated with some ultimate stress, then this occurs when S_r is substantially in excess of unity. Figure 11 also shows the results of the edge-cracked square plate analysis of [5]. In this case, the load normalised by the general yield load (τ/τ_{GY}, see Table 1 of [5]), is converted to the present "flow" based normalisation by multiplying by $2\mathcal{O}_0/(\mathcal{O}_y + \mathcal{O}_u) = 0.61$. It is not surprising that this diagram lies above that for the DPS, beyond general yield, because of the steeper strain hardening assumed in the former ($n = 3$).

In engineering applications, K_r is interpreted as K/K_i where K is the LEFM stress intensity and K_i is the critical/initiation toughness. Thus, a post-yield structural assessment can be made using only the LEFM fracture parameter, K. The usefulness of the assessment diagram method derives from the assumption that the diagram is, at least

Table 3. Tabulation of assessment diagram

s_r	K_r
0.093	0.998
0.275	0.974
0.394	0.927
0.492	0.866
0.569	0.801
0.627	0.739
0.670	0.679
0.701	0.628
0.743	0.546
0.786	0.477
0.840	0.429
0.886	0.387
0.911	0.364
0.936	0.343

roughly, geometry independent. A major feature in ensuring this is a suitable choice of normalising parameter for the abscissa.

7. Conclusion

The results of Section 5 have shown that, for the mode II specimen analysed, the crack tip fields are uniquely determined by the parameter J, and are consistent with the corresponding HRR fields [10]. Since the DPS provides a simple, practical mode II toughness test in the postyield regime, as demonstrated by Green and Miles, [4], the evidence provided by the present analysis that such toughness data are valid is clearly of some interest. The main proviso is that validity has only been demonstrated for,

$$(W-a) \geqslant 76\, J/\tau_0.$$

This is because convergence problems prohibited analysis of larger loads, not because any deviation from J controlled behaviour was found. Nevertheless, our analysis has extended significantly into the post-yield regime, the maximum applied displacement being more than 6 times that to cause general yielding. In this context one may recall that the limit of validity for centre cracked panels in tension (i.e. $W-a \sim 200\ J/\mathcal{O}_0$) occurs prior to

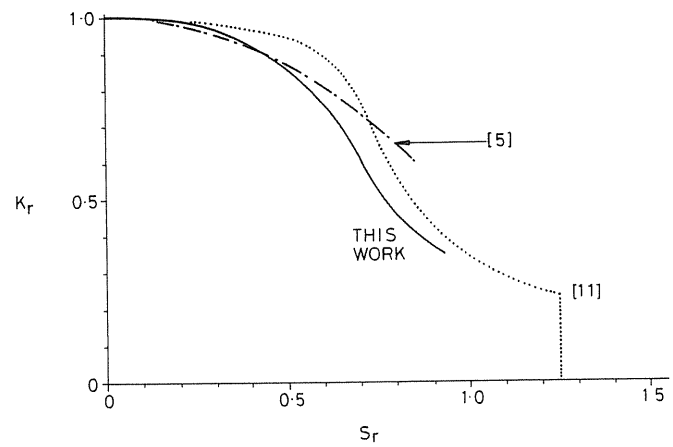

Figure 11. Assessment diagrams.

general yielding, [1,2]. The ASTM E399 criterion for a valid K-test implies that values of $(W-a)\ \tau_0/J$ less than 1440 are significantly yielded. Thus, even the present limited analysis extends substantially the range of valid toughnesses which may be obtained from a given ligament size.

A second proviso is that we have not investigated 3-dimensional effects or attempted to derive validity criteria for the thickness dimension, B. In particular, the effective out-of-plane constraint (plane stress versus plane strain) may vary along the ligament in a 3D analysis. In this respect the situation is identical to that in mode I where only 2D analyses of the near tip fields have been performed (e.g. [1–3]).

The last proviso is that we have considered only one material behaviour, although this is characteristic of carbon-manganese steel rather than a power-law idealisation. In practice, most materials do not conform to power-law behaviour. Most typically the effective hardening index, n (where $\epsilon_p \propto \mathcal{O}^n$) is larger at small strains of a few percent than at large strains. If J-dominance is observed for a large value of n, then it will presumably also occur for smaller n values, i.e the larger hardening index is more onerous to the occurrence of J-dominance (see for example Amazigo [12]). It is desirable, however, to analyse representative materials data since it is not clear whether the effective n value relates to the (high strain) crack tip region or the (smaller strain) far field region.

In addition, we have given in Table 1 the eta factors which relate J to the work done, U, and hence allow mode II toughness measurements to be made simply. Finally, Fig. 11 presents our J results in assessment diagram form, and indicates some mode/geometry dependence of the diagram when compared with the mode I compact tension specimen diagram based on the same materials data, [11].

8. Acknowledgements

The author is grateful to the Director-General of the Central Electricity Generating Board, South Western Region, for permission to publish this paper.

9. References

[1] R.M. McMeeking and D.M. Parks, in *Elastic-Plastic Fracture*, ASTM STP 668 (1979) 175–194.
[2] C.F. Shih and M.D. German, *International Journal of Fracture* 17 (1981) 27–43.
[3] A. Needleman and V. Tvergaard, "Crack Tip Stress and Deformation Fields in a Solid with a Vertex on its Yield Surface", US Department of Energy Contract DE-AC02-80-ER10556, Technical Report 87, Brown University (1981).
[4] G. Green and L. Miles in *Elastic-Plastic Fracture*, Second Symposium, Vol. 1, ASTM STP 803 (1983) 458–479.
[5] R. Bradford, *International Journal of Fracture* 26 (1984) 85–98.
[6] T.K. Hellen, in *Second International Conference on Numerical Methods in Fracture Mechanics*, Swansea, Pineridge Press (1980) 401–415.
[7] J.W. Hutchinson, *Journal of the Mechanics and Physics of Solids* 16 (1968) 13–31, 337–347.
[8] J.R. Rice and G.F. Rosengren, *Journal of the Mechanics and Physics of Solids* 16 (1968) 1–12.
[9] R. Bradford, *International Journal of Fracture* 25 (1984) R7–R9.
[10] C.F. Shih, Ph.D. thesis, "Elastic-Plastic Analysis of Combined Mode Crack Problems", Harvard University, Cambridge, Massachusetts (1973).
[11] R. Bradford, R.S. Gates, G. Green and D.C. Williams, *International Journal of Pressure Vessels and Piping* 19 (1985) 83–99.
[12] J.C. Amazigo, *International Journal of Solids and Structures* 11 (1975) 1291–1299.

Résumé

On recourt au programme d'étude par éléments finis élastoplastiques BERSAFE phase 3 pour analyser le comportement de l'éprouvette au cours de l'essai de double poinçonnement. On étudie la validité des ténacités en mode II obtenus à l'aide de cette éprouvette dans le cas de mises en charge conduisant à plastification généralisée

et au-delà, en examinant les domaines voisins de l'extrémité des entailles où l'intégrale J est prédominante. Ces régions sont établies conformes aux régions à singularités de Hutchinson, Rice, Rosengren en mode II. En outre, on trouve les facteurs de corrélation liant J au travail U appliqué à l'éprouvette, ce qui procure le moyen le plus simple de mesurer une ténacité par voie expérimenale. Enfin, les calculs de J sont exprimés sous forme d'abaque, bien que l'on n'en ait pas étudié l'application à des géométries de constructions. On suppose, dans les analyses faites, que le bridage en un état plan de tension et les données tention-dilatation correspondent à un acier au C-Mn.